


---

# APPROXIMATE BAYESIAN COMPUTATION BASED ON MAXIMA WEIGHTED ISOLATION KERNEL MAPPING

---

A PREPRINT

 **Iurii S. Nagornov** \*

NEC-AIST AI Cooperative Research Laboratory,  
Artificial Intelligence Research Center,  
The National Institute of Advanced Industrial Science and Technology  
iurii.nagornov@aist.go.jp

February 1, 2022

## ABSTRACT

**Motivation:** The branching processes model yields unevenly stochastically distributed data that consists of sparse and dense regions. The work tries to solve the problem of an precise evaluation of a parameter for this type of a model. The application of branching processes model to cancer cell evolution has many difficulties like high dimensionality and rare appearance of a result of interest. Moreover we would like to solve the ambitious task of obtaining the coefficients of the model reflecting the relationship of driver genes mutations and cancer hallmarks on the basis of personal data of variant allele frequencies.

**Results:** The Approximate Bayesian computation method based on Isolation kernel is designed. The method includes a transformation row data to a Hilbert space (mapping) and measure the similarity between simulation points and maxima weighted Isolation kernel mapping related to observation point. Also, we designed heuristic algorithm to find parameter estimation without gradient calculation and dimension-independent. The advantage of the proposed machine learning method is shown for multidimensional test data as well as for an example of cancer cell evolution.

**Keywords** Bayesian inference · Isolation Kernel · Maxima Weighted Mapping · Cancer cell evolution

## 1 Introduction

**Problem definition and motivation.** The paper tries to attack the problem of an as precise as possible evaluation of a parameter for a stochastic model corresponding to branching processes. A branching process is a stochastic process, which consists of collections of random variables indexed by the natural numbers and they are often used for describing a mathematical model of a population Jagers (1989) and Athreya and Ney (2012), for example, the genetic drift in the population genetics Burden and Simon (2016) Chen *et al.* (2017). In contraction to the statistical approach, the branching processes allow to study of dynamics of cell evolution, and this approach is very popular in cancer cell evolution research West *et al.*, 2016. Particular in cancer cell evolution and branching processes in general, ultimate extinction of a population occurs in many cases Devroye (1998). That's why for the initial uniform distribution of parameters, the branching processes model yields unevenly distributed data that consists of sparse and dense regions.

Another problem in the parameter estimation task of branching processes model is the stochastic character of data, especially for cancer cell evolution Nagornov *et al.* (2021). Simulation, based on a model of cell mutations, population evolution and tumor/cancer subpopulations, mainly leads to the emergence of many clones and rarely to the appearance of cancer cells. The ambitious task of obtaining the coefficients of the model reflecting the relationship of driver genes mutations and cancer hallmarks on the basis of personal data of variant allele frequencies (VAFs) is defined in the work

---

\*adress: 2-4-7 Aomi, Koto-ku, Tokyo 135-0064, Japan

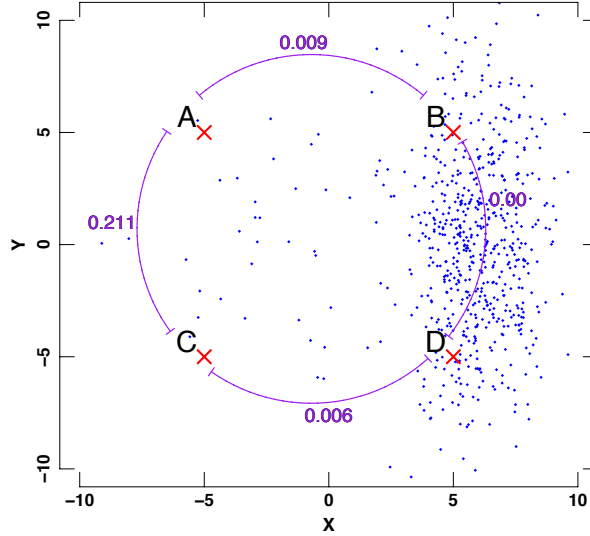


Figure 1: Demonstration of dependence of Isolation Kernel on density of a two-dimension dataset represented by points. The crosses A,B,C and D are points equally distant:  $d_{AB} = d_{BD} = d_{CD} = d_{AC}$ . The right region is dense, the left one is sparse. Arcs with numbers show the similarities between points.

Nagornov and Kato (2020). The solving this challenging problem with precise parameter will give a possibility of a personal predictions of the development of cancer when a certain mutated gene is blocked by a drug. Thus, to obtain model parameters that reflect the personal characteristics of cancer evolution, it is necessary to develop a method for their assessment based on rare events and extremely unevenly distributed stochastic simulation data.

**Proposal of a decision.** Approximate Bayesian computation (ABC) is a well-known approach to get an estimation of the model's parameter under given observation Csillery *et al.* (2010). For example, in the work Williams *et al.*, 2018 to quantify the subclonal selection, ABC was applied to the observation data of VAFs at the genome level in multiple cancers. Unfortunately, rejection ABC gives inaccurate estimation for unevenly distributed data in a multidimensional space of parameters Nakagome *et al.* (2013). The precise estimation of parameter value lying in the sparse region is problematically due to a large scatter of data. So, our proposal is an usage of a machine learning method combined with ABC to improve an accuracy. It is safe to claim that Isolation Kernel is the most appropriate method for this class of the problem because of its unique properties Ting *et al.*, 2020.

Isolation Kernel (iKernel) is proposed in the paper Ting *et al.*, 2018 where the support vector machine problem is decided for multidimensional case more successful rather than other methods. The advantages of iKernel are low computational cost Ting *et al.*, 2020, a possibility to be strong against the curse of dimensionality Ting *et al.*, 2021 and the most interesting that Isolation Kernel is data-dependent. That means that the similarity between two data points depends on the density of the dataset around these points (here and later by similarity we mean the similarity calculated using iKernel if another is not noted).

To demonstrate last property let consider the unevenly distributed data with a sparse and dense regions (Fig. 1). Let select four points equally distant within these two regions - A,B,C and D. Skipping the algorithm of calculation of the similarity  $s \in [0, 1]$ , let us just show calculation of  $s$  between different points: for B and D  $s_{BD} = 0$  in dense area, in contrast to this the  $s_{AC}$  is large with value 0.211 that is close enough to 1 ( $s = 1$  means identity points). The similarity between points from different areas are very small but is not zero ( $s_{AB} = 9 \cdot 10^{-3}$  and  $s_{CD} = 6 \cdot 10^{-3}$ ). Thus, the similarity includes the inverse distance as well as number of neighbor points and this property is used in ABC based on Isolation Kernel mapping.

That's important to consider principles of feature mapping for proposed method, that's why we describe a kernel mapping in Background section. In total the paper has three additional sections: the first one is devoted to background of research with brief overview of kernel methods and specific properties of feature mapping and kernel ABC; the second section is devoted to proposed method ABC based on Isolation Kernel and Voronoi diagram where we define maxima weighted iKernel

mapping; also this section has a description of a heuristics algorithm to get an parameter estimation; and, finally, we show some multidimensional synthetic examples and an application of the method to specific problem of parameter estimation of a simulator of the cancer cell evolution.

## 2 Background

### 2.1 Nonlinear feature map

The kernel function has become popular in the machine learning (ML) field because of the improving of many statistical inference methods Gretton *et al.*, 2012 and Fukumizu *et al.*, 2008. The ML tasks get success under critical condition on the accuracy of the estimation of the data-generating process and kernel methods allow to improve an accuracy and reproducibility of this process Muandet *et al.*, 2017. The general idea of the kernel method is to transform real data  $x \in \mathcal{X}$  to Hilbert space where a similarity measure is used instead of the distance. The similarity measure is usually non-linear and much more flexible Fukumizu *et al.*, 2013, for example, similarity does not obey the rule of the triangle inequality in opposite with the distance metrics.

Another basic part of kernel method is a Hilbert space  $\mathcal{H}$  that is a vector space with an inner product in it  $\langle \cdot, \cdot \rangle$  and feature transformation from real data  $\phi(x) : \mathcal{X} \rightarrow \mathcal{H}$  also called mapping Muandet *et al.*, 2017. Hilbert space has usually dimensionality  $d_{\mathcal{H}}$  much higher than dimension  $d$  of the original real data space  $\mathcal{X}$ .

The inner product plays role the similarity measure function in  $\mathcal{H}$  and it is represented by kernel function such that  $k(x, y) = \langle \phi(x), \phi(y) \rangle$  for any points  $x, y \in R^d$  and  $\phi(x), \phi(y) \in \mathcal{H}$  with dimension  $d_{\mathcal{H}}$  Muandet *et al.*, 2017. For ML the kernel is chosen as the positive definite function and symmetric, i.e.  $k(x, y) = k(y, x)$  Fukumizu *et al.*, 2013. The positive definiteness is a necessary condition to choose the kernel. That's important to note that all kernels based on distances are positive definite and symmetric.

The feature mapping includes the data transformation with increasing dimensionality  $d_{\mathcal{H}} \gg d$  and, in principle, dimension of Hilbert space can be infinity  $d_{\mathcal{H}} = \infty$ , for example as it is for Laplacian and Gaussian kernels. That's why the explicit calculation of  $\phi(x)$  is usually a very tough or impossible computational task. Thus, the most attractive in the usage of kernel methods is that they avoid the explicit calculation of  $\phi(x)$  and use only kernel function instead. This procedure is called a kernel trick that is a very convenient, efficient and accurate algorithm Muandet *et al.*, 2017. So, one can calculate the similarity between all data points in the form of a Gram matrix that is also positive definite and it's defined as follow:

$$G = \begin{pmatrix} k(x_1, x_1) & \cdots & k(x_1, x_n) \\ \vdots & \ddots & \vdots \\ k(x_n, x_1) & \cdots & k(x_n, x_n) \end{pmatrix} \quad (1)$$

For ML they use a reproducing kernel Hilbert space (RKHS) with reproducing kernel which has the reproducing property:

$$f(x) = \langle f, k(\cdot, x) \rangle \quad (2)$$

for any function  $f(x) \in \mathcal{H}$  and any point  $x \in R^d$  where dot in  $k(\cdot, x)$  means all possible points in a Hilbert space. There is a one-to-one correspondence between the reproducing kernel  $k$  and the RKHS  $\mathcal{H}$  (Theorem 2.5 in review Muandet *et al.*, 2017):

**Theorem 1** *For every positive definite function  $k(\cdot, \cdot)$  on  $\mathcal{X} \times \mathcal{X}$  there exists a unique RKHS with  $k$  as its reproducing kernel. Conversely, the reproducing kernel of an RKHS is unique and positive definite.*

For RKHS the feature function can be derived as follow:

$$\phi(x) = k(\cdot, x) \quad (3)$$

and it's called as a canonical feature map. Kernel methods can be used with feature mapping of distributions what is needed in ABC method.

### 2.2 Kernel mean embedding

Kernel methods were extended from points transformation to distributions mapping Bishop, 2006. Row data points  $x \in R^d$  can be considered as distribution  $P(x)$  in real space. The data points can be embedded to a feature space as a distribution in such a way that kernel mean embedding will represent

the distribution in RKHS. For this purpose, the probability space is used as a triplet  $\{\Omega, \Sigma, P\}$ , where  $\Omega$  is the sample space,  $\Sigma \subseteq 2^\Omega$  is sigma algebra with a subset of power of  $\Omega$ ,  $P \in [0, 1]$  is the probability measure on  $\Sigma$  algebra Wasserman, 2010.

The kernel mean embedding based on a random variable that is described as a measurable function defined on a probability space  $\{\Omega, \Sigma, P\}$  that maps from the sample space  $\Omega$  to the real numbers Wasserman, 2010. Let  $X \subset R^d$  and  $Y \subset R^d$  are two random variables such that  $X : \Omega \rightarrow \mathcal{X}$  and  $Y : \Omega \rightarrow \mathcal{Y}$ . The probabilities defined on  $X, Y$  may be marginal, joint, or conditional Fukumizu *et al.*, 2013. Marginal probabilities  $P(X)$  and  $P(Y)$  are the (unconditional) probabilities of an event occurring. Joint probability  $P(X, Y)$  is the probability of event  $X = x$  and  $Y = y$  occurring. The conditional distribution  $P(Y|X)$  shows the functional relationship between two random variables.

To make a distribution mapping the **kernel mean embedding** is used with  $P$  probability measure in the form Muandet *et al.*, 2017:

$$\begin{aligned} \mu_P &:= \mathbf{E}_P[\phi(X)]_{\mathcal{H}} \\ &= \int_{\mathcal{X}} \phi(x) dP(x) \\ &= \int_{\mathcal{X}} k(\cdot, x) dP(x), \end{aligned} \quad (4)$$

where  $k(\cdot, x)$  is a kernel on  $\mathcal{X}$ ,  $\mathbf{E}$  is expectation in feature space. If  $P(x)$  is differentiable then  $dP(x) = \rho(x)dx$  and  $\rho(x)$  is a distribution density. For conditional distribution this definition can be rewritten as follow:

$$\begin{aligned} \mu_{P(\cdot|X)} &:= \mathbf{E}_{P(\cdot|X)}[\psi(Y)|X]_{\mathcal{G}} \\ &= \int_{\mathcal{Y}} \psi(y) dP(y|X) \\ &= \int_{\mathcal{Y}} l(\cdot, y) dP(y|X) \end{aligned} \quad (5)$$

where  $l(\cdot, y)$  is a kernel on  $\mathcal{Y}$ . To construct the Hilbert Space Embedding of conditional distribution the two positive definite kernels  $k$  and  $l$  for  $\mathcal{X}$  and  $\mathcal{Y}$  domains respectively should be defined:

$$\begin{aligned} k : \mathcal{X} \times \mathcal{X} &\rightarrow R & \text{and} & & l : \mathcal{Y} \times \mathcal{Y} &\rightarrow R \\ k(\cdot, x) &= \phi(x) \in \mathcal{H} & \text{and} & & l(\cdot, y) &= \psi(y) \in \mathcal{G} \end{aligned} \quad (6)$$

where  $\mathcal{H}$  and  $\mathcal{G}$  are the corresponding reproducing kernel Hilbert spaces. Based on the given sample  $\{x_1, x_2, \dots, x_n\}$  drawn from  $P(x)$ , the estimation of  $\mu_P$  can be derived using the next formula Muandet *et al.*, 2017:

$$\mu_P = \mathbf{E}_P[\phi(X)]_{\mathcal{H}} \approx \frac{1}{n} \sum_{i=1}^n k(\cdot, x_i) \in \mathcal{H} \quad (7)$$

The important condition for kernels  $k(\cdot, x)$  and  $l(\cdot, y)$  is that they should be Bochner integrable or bounded Fukumizu *et al.*, 2013. In practice one can use **characteristic** kernel such that the kernel mean represents the information about the whole distribution  $P(x)$  Muandet *et al.*, 2017.

### 2.3 Kernel Bayes rule

The target of kernel ABC is to estimate the kernel mean of the conditional distribution. Kernel mean representation of distributions allows to get Bayes' equality and then transform that into the feature space Fukumizu *et al.*, 2013:

$$P(Y|X) = \frac{P(X, Y)}{P(X)} = \frac{P(X|Y) \cdot P(Y)}{P(X)} \quad (8)$$

Here for two random variables  $X$  and  $Y$  the conditional distributions are denoted as  $P(Y|X)$  for all points of  $X$  and  $P(Y|X = x)$  for certain point  $X = x$ . Using the same denotations as in Eq. 6 the conditional mean embeddings  $\mu_{P(Y|X)}$  and  $\mu_{P(Y|X=x)} = \mu_{P(Y|x)}$  of these distributions are defined as expectations in RKHS Muandet *et al.*, 2017:

$$\begin{aligned} \mu_{P(Y|X)} &: \mathcal{H} \rightarrow \mathcal{G} \\ \mu_{P(Y|X)} &\in \mathcal{H} \times \mathcal{G} \\ \mu_{P(Y|x)} &= \mathbf{E}_{P(Y|x)}[\psi(Y)] \\ &= \mu_{P(Y|X)} k(\cdot, x) \end{aligned} \quad (9)$$

Following these definitions  $\mu_{P(Y|X)}$  is a matrix operator from  $\mathcal{H}$  to  $\mathcal{G}$  and  $\mu_{P(Y|x)}$  is an element in  $\mathcal{G}$ . Thus,  $\mu_{P(Y|x)}$  is the conditional expectation of the feature map of  $Y$  given that  $X = x$  that can be represented as the marginal embedding. The embedding operator  $\mu_{P(Y|X)}$  represents the conditioning operation that gives the result as  $\mu_{P(Y|X=x)}$  i.e. one point from whole set.

To get kernel mean embedding the covariance operators are used in the forms:

$$\begin{aligned} C_{YX} &: \mathcal{H} \rightarrow \mathcal{G} \\ C_{YX} &:= \mathbf{E}_{P(Y,X)}[\psi(Y) \otimes \phi(X)] = \mu_{P(Y,X)} \\ C_{XX} &: \mathcal{H} \rightarrow \mathcal{H} \\ C_{XX} &:= \mathbf{E}_{P(X)}[\phi(X) \otimes \phi(X)] \end{aligned} \quad (10)$$

where  $C_{YX}$  is a cross-covariance operator,  $C_{XX}$  is a covariance operator,  $\otimes$  is a outer product of two vectors,  $\psi(Y) \otimes \phi(X) \equiv \psi(Y) \times \phi^T(X)$ , that gives a result as a matrix with elements  $[\psi(Y) \times \phi^T(X)]_{ij} = \psi(y_i) \times \phi(x_j)$ . From these definitions the Kernel mean embedding can be represented as (Definition 4.1 in Muandet *et al.*, 2017):

$$\begin{aligned} \mu_{P(Y|X)} &= C_{YX} C_{XX}^{-1} \\ \mu_{P(Y|X=x)} &= C_{YX} C_{XX}^{-1} k(\cdot, x) \end{aligned} \quad (11)$$

The most important for our research theorem is as follow (Theorem 4.1 in Muandet *et al.*, 2017):

**Theorem 2** Let  $\mu_\pi \in \mathcal{H}$  and  $\mu_{Q_y} \in \mathcal{G}$  be the kernel mean embeddings of  $\pi$  and  $Q_y$  distributions, respectively. Let  $R(C_{XX})$  denote the range space (span of the column vectors) of a covariance operator  $C_{XX}$ . If  $C_{XX}$  is injective,  $\mu_\pi \in R(C_{XX})$ , and  $\mathbf{E}[\psi(Y)] \in \mathcal{G}$  for any  $\psi \in \mathcal{G}$ , then

$$\begin{aligned} \mu_{Q_y} &= C_{YX} C_{XX}^{-1} \mu_\pi, \\ \mu_\pi &\in \mathcal{H} \\ \mu_{Q_y} &\in \mathcal{G} \end{aligned} \quad (12)$$

In practice the joint distribution  $P(X, Y)$  is unknown that's why they cannot compute  $C_{XX}$  and  $C_{YX}$  directly. Empirical estimation of  $\mu_{Q_y}$  is based on the sample  $(x_1, y_1), \dots, (x_n, y_n)$  from  $P(X, Y)$  which is arising from independent and identically distributed random variables  $X$  and  $Y$ . Then the conditional mean embedding  $\mu_{P(Y|X=x)}$  can be estimated using (Theorem 4.2 in Muandet *et al.*, 2017):

$$\begin{aligned} \mu_{P(Y|X=x)} &\approx \Psi(\mathbf{G} + n\lambda\mathbb{I}_n)^{-1} \Phi^T k(\cdot, x) \\ \Psi^T &:= [\psi(y_1), \psi(y_2), \dots, \psi(y_n)]^T \\ \Phi^T &:= [\phi(x_1), \phi(x_2), \dots, \phi(x_n)]^T \\ \mathbf{G} &= \Phi^T \Phi \end{aligned} \quad (13)$$

where  $\mathbf{G}$  is a Gram matrix in  $\mathcal{H}$ ,  $\mathbb{I}_n$  is identity matrix of rank  $n$ , and  $\lambda$  is a positive regularization constant.

## 2.4 Kernel ABC

In the rejection ABC, to get the posterior distribution it iteratively generates a lot of simulations, gets summary statistics for each simulation to reduce a dimension of a problem and finally decides on rejection or acceptance of the simulation Kajihara *et al.*, 2018; Csillery *et al.*, 2010. Accepted simulations give us a posterior distribution of parameters where maximum a posterior is usually used as parameters' estimation for the given observation. In kernel ABC an element of RKHS space represents a distribution, so we need not use summary statistics in principle. The maximum mean discrepancy MMD criterion is used to check the consistency of the distributions of observation and simulation data instead Park *et al.*, 2016. The target of kernel ABC is to get kernel mean embedding of posterior distribution using the formulation of Eq.(13), and then to generate a sampling using the complementary algorithm like kernel herding Chen *et al.*, 2010. Finally, the parameter estimation can be got based on the posterior distribution of new sampling. To carry out the kernel ABC, the definition of a model, observation and simulation data as well as RKHS are needed.

Let us assume a stochastic model which has a measurable variable  $\Theta \in \mathcal{Q}$  as an input  $d$ -dimension parameter and, the results of the model's simulation are represented by another measurable variable

$S \in \mathcal{S}$  of  $d_s$  dimension. The  $\mathcal{Q}$  and  $\mathcal{S}$  are corresponding domains. Note that the result is not deterministic due to the stochastic nature of the simulation. Let consider an observation point  $s^* \in \mathcal{S}$  and given sample of  $n$  simulations  $S = \{s_1, s_2, \dots, s_n\} \in \mathcal{S}$  based on related input parameters  $\Theta = \{\theta_1, \dots, \theta_n\} \in \mathcal{Q}$ . The corresponding prior distributions of parameters  $\pi(\theta)$  and simulations  $P(s)$  are given by:

$$\begin{aligned} S &= \{s_1, s_2, \dots, s_n\} \in \mathcal{S} \\ \Theta &= \{\theta_1, \dots, \theta_n\} \in \mathcal{Q} \\ s &\sim P(s) \\ \theta &\sim \pi(\theta) \end{aligned} \quad (14)$$

Therefore, the posterior distribution  $P(\theta|s^*)$  of the parameters  $\theta$  on given observation  $s^*$  can be obtained from Eq. (8) in the form:

$$P(\theta|S = s^*) \propto P(s^*|\theta) \cdot \pi(\theta), \quad (15)$$

where  $P(s, \theta)$  is a joint distribution of  $s$  and  $\theta$ ,  $P(s|\theta)$  is a conditional distribution. In the kernel ABC, the kernel mean embedding of the posterior distribution  $P(\theta|S = s^*)$  is defined as follow Park *et al.*, 2016 and Kajihara *et al.*, 2018:

$$\mu_{P(\theta|S=s^*)} = \int_{\mathcal{Q}} l(\cdot, \theta) dP(\theta|s^*) \in \mathcal{G} \quad (16)$$

where  $l(\cdot, \theta) \in \mathcal{G}$  denotes the kernel in reproducing kernel Hilbert space  $\mathcal{G}$ . In order to exploit the Eq. (16) one must define two kernels:  $l(\cdot, \theta)$  for domain of parameters  $\mathcal{Q}$  and  $k(\cdot, s)$  for domain of simulations  $\mathcal{S}$ :

$$\begin{aligned} k : \mathcal{S} \times \mathcal{S} &\rightarrow R & \text{and} & \quad l : \mathcal{Q} \times \mathcal{Q} \rightarrow R \\ k(\cdot, s) &= \phi(s) \in \mathcal{H} & \text{and} & \quad l(\cdot, \theta) = \psi(\theta) \in \mathcal{G}, \end{aligned} \quad (17)$$

where  $\mathcal{H}$  is reproducing kernel Hilbert space for  $k(\cdot, s)$ ,  $\phi(s)$  and  $\psi(\theta)$  are mapping function for  $\mathcal{H}$  and  $\mathcal{G}$  respectively. Keeping the same denotation we can rewrite Eq. (13) replacing  $X, Y$  with  $S, \Theta$  and  $x, y_i$  with  $s^*, \theta_i$  Muandet *et al.*, 2017:

$$\begin{aligned} \mu_{P(\theta|S=s^*)} &\approx \Psi(\mathbf{G} + n\lambda\mathbb{I}_n)^{-1} \Phi^T k(\cdot, s^*), \\ \Psi^T &:= [\psi(\theta_1), \psi(\theta_2), \dots, \psi(\theta_n)]^T \\ \Phi^T &:= [\phi(s_1), \phi(s_2), \dots, \phi(s_n)]^T \\ \mathbf{G} &= \Phi^T \Phi \end{aligned} \quad (18)$$

To exemplify numerical calculation with  $\Psi$  and  $\Phi$  let define the dimensions of the Hilbert spaces  $\mathcal{H}$  and  $\mathcal{G}$  as  $d_\phi$  and  $d_\psi$ . Then Gram matrix  $\mathbf{G} \in R^{n \times n}$  can be represented as  $n \times n$  matrix,  $\Psi \in R^{d_\psi \times n}$  can be represented as  $d_\psi \times n$  matrix and  $\Phi$  is similar. Thus, Gram matrix can be explicitly rewriting as Muandet *et al.*, 2017 and Gelb *et al.*, 2021:

$$\mathbf{G} := \begin{pmatrix} k(s_1, s_1) & \cdots & k(s_1, s_n) \\ \vdots & \ddots & \vdots \\ k(s_n, s_1) & \cdots & k(s_n, s_n) \end{pmatrix} \in R^{n \times n} \quad (19)$$

Because of  $k(\cdot, s^*) = \phi(s^*) \in R^{d_\phi}$  that is  $d_\phi \times 1$  matrix, and  $\Phi^T \in R^{n \times d_\phi}$  can be represented as  $n \times d_\phi$  matrix, that's why the result of  $\Phi^T k(\cdot, s^*)$  is a  $n \times 1$  matrix Gelb *et al.*, 2021:

$$\begin{aligned} \Phi^T k(\cdot, s^*) &= [\phi(s_1), \phi(s_2), \dots, \phi(s_n)] \phi(s^*) \\ &= [\phi(s_1)\phi(s^*), \phi(s_2)\phi(s^*), \dots, \phi(s_n)\phi(s^*)]^T \\ &= [k(s_1, s^*), k(s_2, s^*), \dots, k(s_n, s^*)]^T \in R^{n \times 1} \end{aligned} \quad (20)$$

Also,  $(\mathbf{G} + n\lambda\mathbb{I}_n)^{-1} \in R^{n \times n}$  is a matrix  $n \times n$ , therefore the result of  $\mathbf{w} = (\mathbf{G} + n\lambda\mathbb{I}_n)^{-1} \Phi^T k(\cdot, s^*) = (w_1, w_2, \dots, w_n)^T \in R^{n \times 1}$  is represented as the weights that is a matrix

of  $n \times 1$ . Usually, the Eq. (18) is written as a sum of multiplications of the weights  $\mathbf{w}$  and feature mapping  $l(\cdot, \theta_i) = \psi(\theta_i), i \in [1, n]$  Muandet *et al.*, 2017:

$$\begin{aligned} \mu_{P(\theta|S=s^*)} &\approx \Psi(\mathbf{G} + n\lambda\mathbb{I}_n)^{-1}\Phi^\top k(\cdot, s^*) \\ &= \Psi \times \mathbf{w} \\ &= \sum_{i=1}^n w_i \psi(\theta_i) \in \mathcal{G} \end{aligned} \quad (21)$$

Under conditions of  $n \rightarrow \infty$  and  $\lambda \rightarrow 0$ , the estimation will converge to true-value consistently Fukumizu *et al.*, 2013 and Muandet *et al.*, 2017.

### 3 ABC based on Maxima Weighted Isolation Kernel mapping

#### 3.1 Isolation Kernel

Isolation Kernel (iKernel) was proposed in the paper Ting *et al.* (2018) and it is based on Isolation Forest (iForest) algorithm Liu *et al.* (2008) (see details in Application 1). The formal definition of Isolation Kernel is as follow Ting *et al.* (2018):

- Let  $D = \{x_1, \dots, x_n\}$ ,  $x_k \in R^d$  be a dataset sampled from an unknown probability density function  $x_k \sim \mathcal{P}_D$ .
- Moreover, let  $H_\xi(D)$  denote the set of all partitions  $H$  that are admissible from the dataset  $\mathcal{D} \subset D$  where each point  $z \in \mathcal{D}$  has the equal probability of being selected from  $D$ ; and  $|\mathcal{D}| = \xi$ . Other words subset  $\mathcal{D} = \{z_1, z_2, \dots, z_\xi\}$  was extracted from initial set  $D = \{x_1, \dots, x_n\}$  ( $\xi \ll n$ ) in order to make partitions  $H_\xi(D)$ .
- Each isolating partition  $\eta[z] \in H_\xi$  isolates one point  $z \in \mathcal{D}$  from the rest of the points in a random subset  $\mathcal{D}$ ,  $\xi$  is number of elements in the subset  $\mathcal{D}$ .
- In the Definition 2.1 of paper Ting *et al.* (2020) they defined:

**Definition 1** For any two points  $x, y \in R^d$ , Isolation Kernel of  $x$  and  $y$  is defined to be the expectation taken over the probability distribution on all partitionings  $H \in H_\xi(D)$  that both  $x$  and  $y$  fall into the same isolating partition  $\eta[z] \in H$ , where  $z \in \mathcal{D}, \xi = |\mathcal{D}|$ :

$$\begin{aligned} k_I(x, y|D) &= \mathbb{E}_{H_\xi(D)}[\mathbf{1}(x, y \in \eta[z]|\eta[z] \in H)] \\ &= \mathbb{E}_{\mathcal{D} \in D}[\mathbf{1}(x, y \in \eta[z]|z \in \mathcal{D})] \\ &= P(x, y \in \eta[z]|z \in \mathcal{D} \subset D), \end{aligned} \quad (22)$$

where  $\mathbf{1}(B)$  is the indicator function which outputs 1 if  $B$  is true; otherwise,  $\mathbf{1}(B) = 0$ . Equation (4) in paper Ting *et al.* (2020) provides how to calculate Isolation Kernel in practice with approximation for finite number of partitionings:

$$\begin{aligned} k_I(x, y|D) &\approx \frac{1}{t} \sum_{i=1}^t \mathbf{1}(x, y \in \eta|\eta \in H_i) \\ &\approx \frac{1}{t} \sum_{i=1}^t \sum_{\eta \in H_i} \mathbf{1}(x \in \eta) \mathbf{1}(y \in \eta) \\ &\approx \frac{1}{t} \Phi^\top(x) \times \Phi(y), \end{aligned} \quad (23)$$

where  $\Phi(x)$  is feature mapping of  $x$ . In accordance with Definition 3.1 in paper Ting *et al.* (2020) the feature mapping  $\Phi(x) : x \rightarrow \{0, 1\}^{t \times \xi}$  of  $k_I$  is a vector that represents the partitions in all the partitioning  $H_i \in \mathbb{H}_\xi(D), i = [1, t]$ ; where  $x$  falls into only one of the  $\xi$  partitions in each partitioning  $H_i$ .

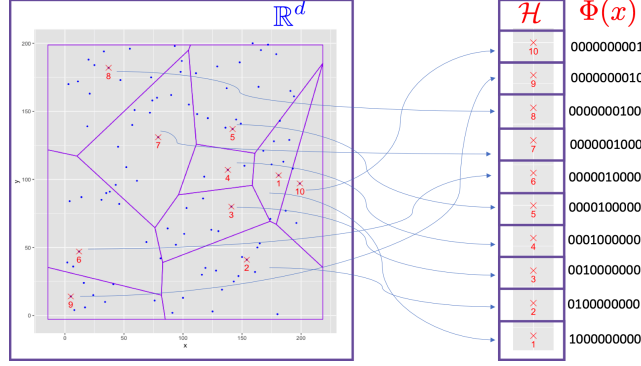


Figure 2: An illustration of feature map  $\Phi(x)$  of Isolation Kernel for the only partitioning of ten partitions. Each partition relates to a point (as red cross)  $z \in \mathcal{D}$  where  $|\mathcal{D}| = \xi = 10$  are randomly selected from the given dataset  $D$ . When a point  $x_i$  falls into a partition region  $\eta[z_j]$ ,  $x_i$  is regarded to be in the related point in  $\mathcal{H}$  space and coding by feature map  $\Phi(x_i)$ .  $\Phi(x_i)$  is a binary vector with a single '1' which position corresponds to number of partition.

The accuracy of the approximation is estimated for iTree method of partitioning in paper Ting *et al.* (2018) and represented as approximating the probability distribution of two points of  $\delta$ -distance falling into the same isolating partition:

$$k_I(x, \delta) \approx \xi^{-\varkappa\delta}, \quad (24)$$

where  $\varkappa \leq 0$  is an integer indicating the multiplies of  $\delta$  from  $x$ . The  $\xi$  plays the role of sharpness and with increasing of  $\xi$  the resolution of Isolation Kernel also is improved. The upper boundary for  $\xi$  is the condition  $\xi \ll n$  in order to keep diversity of partitionings. The last parameter  $t$  can be chosen from the reason of computational cost because with increasing number of trees we can improve accuracy, but other hand it increases the computational time.

Isolation Kernel is positive definite is a quadratic form and Isolation Kernel defines a RKHS  $\mathcal{H}$  Ting *et al.* (2020). The isolation partitioning mechanisms which can be used to implement Isolation Kernel are iForest, Voronoi diagram Ting *et al.* (2018) or newly proposed method based on hyperspheres Ting *et al.* (2020). The iForest requires choosing several issues in an iteration: firstly, a subset  $\mathcal{D}$  of points  $\{z_1, \dots, z_\xi\}$ , then choosing a dimension with a point for the splitting of multidimensional space  $R^d$ , and finally, construct many *iTrees*. So, the time consuming of training stage is proportional to  $O(\xi \times \log_2 \xi \times t)$ . The Evaluation stage is needed to compute the length of *iTree* for each data point  $x \in D$  using recursive function Ting *et al.* (2020). That's why for this case the computational cost will be  $O(\log_2 \xi \times t)$  for each new point.

### 3.2 Isolation Kernel based on Voronoi diagram

Let's consider the algorithm of Isolation Kernel based on Voronoi diagram Ting *et al.* (2020). In the simplest two dimensional case, a Voronoi diagram is a partition of a plane into regions close to each of a given set of points (called Voronoi sites or seeds) Fortune (1987), Wan *et al.* (2019). For each site, there is a corresponding region, called Voronoi cell, consisting of all points of the plane closer to that site than to any other Aurenhammer and Edelsbrunner (1984), Huang *et al.* (2020). Fig. 2 shows an example of partitioning using Voronoi diagram. Voronoi sites are shown with numbered red crosses. The Voronoi cells are represented as polygons dividing all the plane. The advantage of Voronoi diagram is in a very simple method of dividing all points into cells by just calculating distances and choosing the minimal one.

The algorithmic steps of feature mapping  $\Phi(x)$  using Voronoi diagram are presented in Algorithm 1, and the data transformation is shown in Fig. 2. The algorithm to calculate feature mapping  $\Phi(x)$  for each point  $x$  in dataset  $D = \{x_1, x_2, \dots, x_n\} \in R^d$ , where  $d$  is dimension,  $t$  is a number of partitionings. For each partitioning  $\mathcal{H}_i$  the number of partitions is fixed and equals  $\xi$  and the value of feature mapping for each point  $x$  equals  $\Phi_i(x)$  which is binary vector with just one 1 and all zeros in



other positions that represents fact that  $x$  falls into either only one partition in each partitioning  $H_i$ . The feature mapping is achieved by concatenation of all  $\Phi_i(x)$ .

---

**Algorithm 1:** Algorithm to calculate feature mapping  $\Phi(x)$

---

**Input:** Dataset  $D = \{x_1, x_2, \dots, x_n\} \in R^d$

**for**  $i = 1 \dots t$  **do**

**begin**

**Make partitioning**  $\mathcal{H}_i$ :

    Randomly get subset  $\mathcal{D}_i \subset D$ , where  $\mathcal{D}_i = \{z_{i1}, z_{i2}, \dots, z_{i\xi}\}$

    Get Voronoi diagram with partitions  $\mathcal{H}_i$  and

    corresponding Voronoi cells  $\{V_{ik}(z_{ik})\}, k \in [1, \xi]$

**end**

**foreach**  $x \in D$  **do**

**foreach**  $\eta_j \in \mathcal{H}_i, j = 1 \dots \xi$  **do**

      Calculate  $\Phi_{ij}(x) = \mathbf{1}(x \in \eta_j | \eta_j \in \mathcal{H}_i)$

    Calculate  $\Phi_i(x) = [0000\dots 1\dots 000]$  where position of 1 corresponds to Voronoi cell  $v_i(x) \in \{V_{ik}(z_{ik})\}$  which  $x$  belongs

**Result:**  $\Phi(x) = \text{concatenation } \{\Phi_1(x), \dots, \Phi_t(x)\}$

**Output:**  $\{\mathcal{D}_i\}, \{\mathcal{H}_i\}, \{v_i(x)\}, \{V_{ik}(z_{ik})\}, i \in [1, t], k \in [1, \xi]$

---

The partitioning is implemented as follow: firstly, choose from original dataset  $D$  the sites  $z_j \in \mathcal{D}, j = [1 \dots \xi]$  that define partitions  $\eta[z_j]$  (Fig. 2). For each point  $x_i \in D$  we can determine to which partition this point  $x_i$  belongs calculating the distances to all points  $z \in \mathcal{D}$  and choosing minimal one. In this manner we can separate all points  $x_i$  and reflect them into feature map  $\Phi(x_i)$  as binary number of each partition which has a single '1' at a position corresponds to number of partition. This mechanism has been shown to produce large partitions in a sparse region and small partitions in a dense region Ting *et al.* (2020).

Voronoi diagram requires a subset of  $\xi$  points for  $t$  Trees at the Training stage, so, the computational cost is evaluated as  $O(\xi \times t)$ . At the Evaluation stage for each new point  $x$  it is needed to find the nearest point from  $x$  to one point of subset  $\mathcal{D} = \{z_1, \dots, z_\xi\}$ , so, it's needed to find  $\xi$  distances. Making this calculation for each tree, we can estimate time consuming as  $O(\xi \times t)$  which is a same order of cost for Training stage.

### 3.3 The Maxima Weighted iKernel mapping

To get posterior distribution for parameters  $P(\theta|S = s^*)$  under given observation  $s^*$ , it's necessary to generate sampling of  $\theta$  from  $\mathcal{Q}$  (Eqs. 15 and 16). There are many appropriate methods to generate sampling including Kernel Herding Chen and Welling, 2010, Markov Chain Monte-Carlo (MCMC) Dyer *et al.*, 1991, Sequential Monte-Carlo (SMC) Liu and Chen, 1998, Sequential Kernel Herding Lacoste-Julien *et al.*, 2015.

Note that the dimensions  $d_\phi$  and  $d_\psi$  of Hilbert spaces  $\mathcal{H}$  and  $\mathcal{G}$  can be infinite in principle, that's why the kernel trick is used in computations to avoid direct calculation of kernel mean embedding. The common approach to check the convergence is the maximum mean discrepancy MMD that uses the kernel trick as well Borgwardt *et al.*, 2006 and Park *et al.*, 2016. To get initial and generated sampling, they use weights like  $\Phi^T k(\cdot, s^*)$  that is also is based on kernel trick (Eqs. 20 and 21).

As opposed to the kernel trick method we suggest the calculation of the maxima weighted state of the kernel mean embedding  $\mu_{P(\theta|S=s^*)}$  in RKHS  $\mathcal{G}$  explicitly using (Eq.21) with a transformation based on properties of Isolation Kernel (Eqs. 22 and 23) and output of the Algorithm 1. The most important and interesting idea is that we got  $\mu_{P(\theta|S=s^*)}$  in RKHS  $\mathcal{G}$  related to space of parameters, that's why iKernel will give us information about parameter related to observation directly.

Let consider the properties of iKernel from its definition:

- iKernel mapping consists from numerous elements and each element originates from Voronoi diagram.
- Fig. 2 demonstrates that each element in RKHS  $\mathcal{G}$  gives the identification of a Voronoi cell from the whole diagram.
- The number of elements in RKHS  $\mathcal{G}$  is determined by approximation in Eq. 23 and relates to the number of trees  $t$  in the Isolation Forest or number of Voronoi diagrams.

Keeping the denotations of Eq. (14) and in order to prepare iKernel let define Voronoi diagrams using sample of parameters  $\Theta$  with size  $n$  for each tree in accordance with Algorithm 1:

$$\begin{aligned} z_{jk} &\subset \Theta \quad j \in [1, t] \quad k \in [1, \xi] \text{ and } \xi \ll n \\ V_{jk}(z_{jk}) &= \{\theta \in \mathcal{Q} | d(\theta, z_{jk}) \leq d(\theta, z_{pk}), p \neq j\}, \end{aligned} \quad (25)$$

where  $z_{jk}$  is  $k^{th}$  site of the  $j^{th}$  tree or Voronoi diagram which is an element of parameters sample  $\Theta$ , there are  $\xi$  sites in each Voronoi diagram/tree, and  $t$  is a number of trees/Voronoi diagrams,  $V_{jk}(z_{jk})$  is Voronoi cell related to site  $z_{jk}$ ,  $d(\cdot, \cdot)$  is a distance metric.

Next we can define the Isolation Kernel and feature mapping  $l(\cdot, \theta) = \psi(\theta)$  related to Algorithm 1 as follow:

$$\begin{aligned} V_{jk}(z_{jk}) &\xrightarrow{\text{Alg.1}} \psi(\theta) \\ \psi(\theta_i) &\xleftarrow{\text{Alg.1}} \{\zeta_{i1}, \dots, \zeta_{it}\} = \{\zeta_{ij}\} \\ \zeta_{ij} &= \arg \min_{k \in [1, \xi]} d(\theta_i, z_{jk}), \end{aligned} \quad (26)$$

where  $\zeta_{ij}$  is a Voronoi site with a minimal distance to  $\theta_i$  parameter from a set of the sites  $\{z_{jk}\}$  of the  $j^{th}$  Voronoi diagram/tree.

The formula of Eq. (21) gives an information about a contribution from each sample point to the kernel mean embedding of observation point in RKHS  $\mathcal{G}$ . The weights  $\Phi^T k(\cdot, s^*)$  are similarity coefficients between sample points and observation point. So, series of sum in Eq. (21) gives information about Voronoi diagrams in the parameters space through similarity between sample points and observation point in the space of  $S$  - results of simulations. Incorporating Eqs. (21, 25 and 26) together we can describe the iKernel mean embedding  $\mu_{P(\theta|S=s^*)}$  as weighted distribution of Voronoi sites for each  $j^{th}$  tree:

$$\begin{aligned} P_{jk}(z_{jk}) &\iff \mu_{P(\theta|S=s^*)} = \sum_{i=1}^n w_i \psi(\theta_i) \\ P_{jk}(z_{jk}) &\propto \frac{1}{n} \sum_{i=1}^n w_i \times \mathbf{1}(\zeta_{ij} = z_{jk}), \end{aligned} \quad (27)$$

where  $P_{jk}(z_{jk})$  is a probability to find a parameter related to observation  $s^*$  close to  $k^{th}$  Voronoi site  $z_{jk}$  of the  $j^{th}$  tree/diagram.

Now we turn to an algorithm of seeking of the parameter related to observation  $s^*$  using the maxima weighted state of  $\mu_{P(\theta|S=s^*)}$ . This procedure reduces information from iKernel mean  $\mu_{P(\theta|S=s^*)}$  but, other hand, it gives us possibility to find an position in many dimensional space of parameters with high probability related to  $s^*$ . So, our strategy is based on the obvious hypothesis that true value is near by a point related to maxima weighted iKernel mapping. For this purpose let get maxima weighted of the probabilities  $P_{jk}(z_{jk})$  across the trees:

$$\begin{aligned} z_j^* &= \arg \max_{k \in [1, \xi]} P_{jk}(z_{jk}) \\ v_j^* &= v_j(z_j^*) \\ \mu_{v^*} &\xleftarrow{\text{Alg.1}} \{z_1^*, \dots, z_t^*\}, \end{aligned} \quad (28)$$

where  $\{v_1^*, \dots, v_t^*\}$  and  $\{z_1^*, \dots, z_t^*\}$  are Voronoi cells and sites related to the maxima weighted state of  $\mu_{P(\theta|S=s^*)}$  (denoted as  $\mu_{v^*}$ ) of the observation point  $s^*$  in the parameter space  $\mathcal{Q}$ .

After getting the maxima weighted iKernel mapping  $\mu_{v^*}$  in the explicit form of the list of Voronoi cells of trees as well as element of Hilbert space  $\mathcal{G}$ , it's possible to detect the position or tiny area  $v^*$  in the parameter space related to observation with the high probability as intersection of all Voronoi cells:

$$v^* = \bigcap_{j=1}^t v_j^* \quad (29)$$

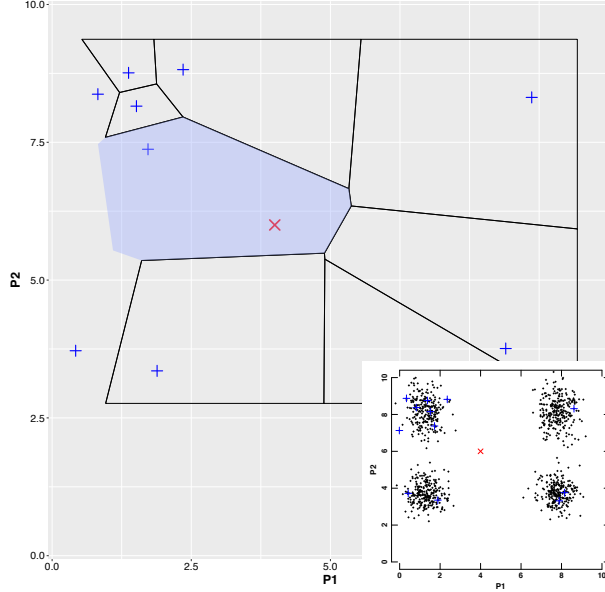


Figure 3: A Voronoi diagram in the parameter space of  $P1$  and  $P2$ : straight crosses are Voronoi sites, partitions related to Voronoi cells, oblique cross is observation point and the shaded area is the Voronoi cell to which observation belongs. **Insert:** There are the points of the sample dataset. The straight crosses are subset of Voronoi sites and oblique cross is observation point.

We have to note that  $v^*$  can be empty set in principle, that's why we do not use the intersection area for calculation and here we use it to demonstrate the algorithmic features of our method and to show an example of a two-dimensional case.

To explain the usage of Eqs. (27, 28 and 29) of Isolation Kernel let consider an example with the unevenly distributed sample data (insert on Fig. 3) of two-dimensional parameters ( $P1$  and  $P2$ ) and getting just twelve sites  $\xi = 12$  and only 5 trees  $t = 5$ . The similar unevenness of the sample data appears under stochastic simulation with frequent null-output in the certain area of parameters space. One may call it "rare events" which usually attracts interest. Also, let carry out the truth observation point into the plots to show how close the algorithm is able to find a decision (oblique cross at Fig. 3 and point at Fig. 4).

Figure 3 demonstrates the example of the Voronoi diagram and Voronoi cell to which the observation point belongs. Iteratively an algorithm finds all Voronoi cells and finally, it is possible to find the intersection  $v^*$  (Eq. 29) of all Voronoi cells from all Voronoi diagrams (Fig. 4). As shown the intersection  $v^*$  of the Voronoi cells is a very small area even for 5 cells or trees. In further calculations, we usually use 20-70 sites and 200-400 trees that are much more than in the example. In the supplementary video, the iterative process is shown with a selection of sites, construction of Voronoi diagram and denotation of intersection.

Thus, the machine learning algorithm of the ABC based on maxima weighted iKernel mapping  $\mu_{v^*}$  consists from several steps:

- Definition of kernel and feature mapping  $k(\cdot, s) = \phi(s) \in \mathcal{H}$  in the space of results of simulation  $\mathcal{S}$  Eqs. (14, 17). Note it can be any type of kernel with reproducing property (it's not necessary iKernel).
- According with Eqs. (19,20) getting Gram matrix  $\mathbf{G}$  and weights  $\Phi^T k(\cdot, s^*)$  of similarity between simulation and observation points.
- **Training step:** Run Algorithm 1 with iKernel  $l(\cdot, \theta) = \psi(\theta) \in \mathcal{G}$  (Eq. 17) to get Voronoi sites ( $z_{jk}$ ) and cells  $V_{jk}(z_{jk})$  (Eqs. 25,26) as well as Voronoi cells  $v_i(\theta)$  (where  $i \in [1, t]$ ) related to all the simulation points in the parameter space  $\Theta = \{\theta_1, \theta_2, \dots, \theta_n\} \in \mathcal{Q}$ .
- Using Eq. (21) to calculate  $\mu_{P(\theta|S=s^*)}$  related to observation point  $s^*$ .
- Using Eqs. (27 and 28) to get maxima weighted iKernel mapping  $\mu_{v^*}$ .
- To find a point or points corresponded to the intersection of the Voronoi cells  $v^*$  (Eq. 29) in the parameter space  $\mathcal{Q}$ .

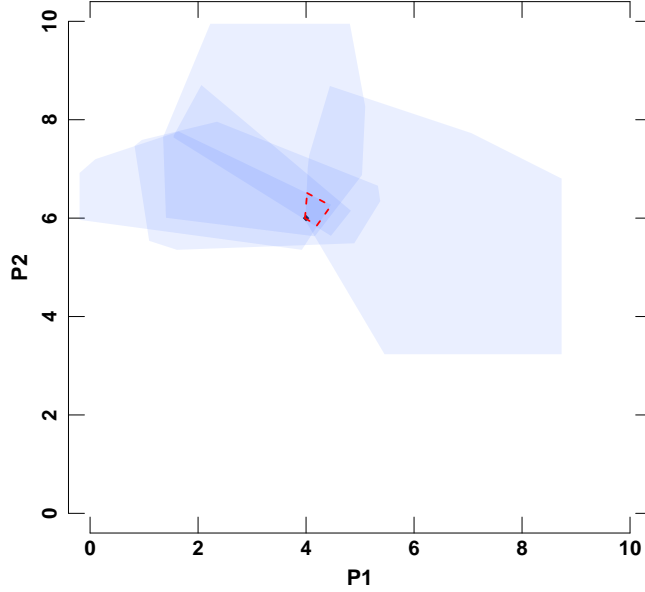


Figure 4: An intersection of the Voronoi cells from different Voronoi diagrams. Voronoi cells are denoted as semi transparent areas and intersection is circled with a dashed line.

Note that the intersection can be empty  $v^* = \emptyset$  in principle, so, to find the corresponding point  $\theta^*$  we use maxima weighted iKernel mapping  $\mu_{v^*}$  in additional algorithm with calculation of similarity measure  $l(\theta, v^*) = \psi(\theta)\mu_{v^*}$ , where  $\theta$  is any parameter. The last step of the proposed algorithm can be implemented using different methods, here we use a heuristic algorithm without claims to the best efficiency and optimality.

### 3.4 Heuristic algorithm 'Tracers'

We would like to construct the algorithm of seeking  $\theta^*$  related to  $\mu_{v^*}$  as an algorithm independent on dimension of the parameters space without calculation of gradient. For this propose we generate points in the parameter space, transform them to the Hilbert space and, finally, measure similarity between their iKernel mapping and maxima weighted iKernel mapping  $\mu_{v^*}$  of the observation point. We call generated points as 'tracer points' because of the association with the tracer bullets in the dark sky, so, the algorithm consists from several steps (Algorithm 2).

At first, to get Voronoi sites  $z_j^*$  ( $j \in [1, t]$ , Eq. 27) from the Algorithm 1 then for each site to find the most distant site  $z_m^*$  and to generate points between these sites called tracer points (Fig. 5):

$$\{\theta_i^{tr}\} = \{\alpha_i \times z_j^* + (1 - \alpha_i) \times z_m^*\} \quad \alpha_i \in [0, 1] \forall i \quad (30)$$

Steps 2 and 3 of Algorithm 2 include the getting the iKernel mapping  $\psi(\theta_i^{tr})$  and calculation the similarity between tracer points and maxima weighted iKernel mapping  $\mu_{v^*}$  (Fig. 5):

$$l(\theta_i^{tr}, v^*) = \psi(\theta_i^{tr})\mu_{v^*} \quad (31)$$

Finally, using the linear regression to the tracer points with  $\Theta_{select} = \{\theta_i^{tr} | l(\theta_i^{tr}, v^*) > 0.5\}$  to get coefficients of the linear regression for each parameter  $\beta = \{\beta_i\}$ , where  $i \in [1, d]$ ,  $d$  is a dimension of the parameter space  $\mathcal{Q}$ . That allows to generate points along a line  $\theta_\tau = \theta_b + \beta \times \tau$ , where  $\tau$  is a new variable to build a straight line and repeat all steps until the similarity (Eq. 31) stops changing with criterion  $\epsilon$ . Algorithm 2 gives the approximate position in the parameter space with the highest value of similarity  $l(\theta_\tau, v^*) = \psi(\theta_\tau)\mu_{v^*}$ .

We have to note that the heuristic algorithm Tracers is independent on dimension of parameter space  $\mathcal{Q}$  and instead the calculation of the gradient (like in gradient descending method) we generate tracer points with calculation of  $l(\theta_i^{tr}, v^*)$  for each tracer  $\theta_i^{tr}$ . That's why this algorithm should be appropriate for multidimensional data as well as for stochastic simulator based on the branching processes. Thus, the heuristic algorithm Tracers in combination with maxima weighted iKernel

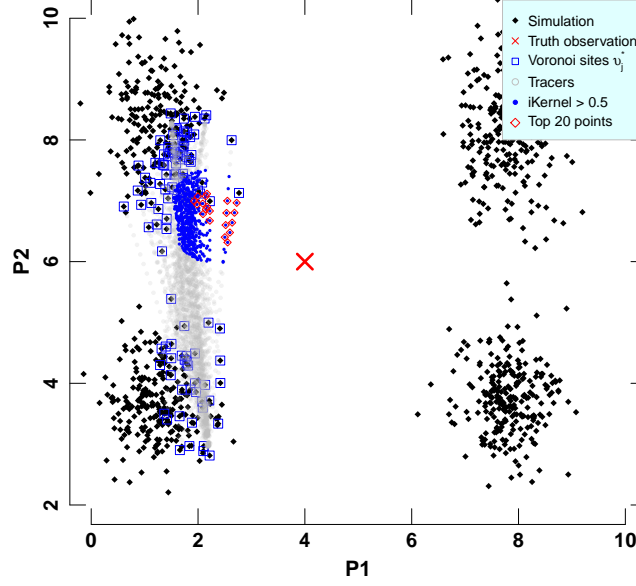


Figure 5: Finding an intersection of the Voronoi cells using tracer points (tracers) generated between Voronoi sites  $v_j^*, j \in [1, t]$  from all the trees/Voronoi diagrams. There are tracer points  $\theta_i^{tr}$  with value of the similarity  $\psi(\theta_i^{tr})\mu_{v^*} > 0.5$  as well as top 20 of these points with the highest similarities.

mapping based on Voronoi diagram gives an approximation parameter for the unevenly distributed sample data getting from the stochastic model. To check the efficiency of the proposed algorithms we used many dimension data of gaussian distributed points with a gap in the center of distribution. Also, to check how the accuracy of an estimated parameter depends on stochasticity of the model we increase the noise part of a simulation.

---

**Algorithm 2:** Heuristic algorithm 'Tracers' to find parameter related to maxima weighted iKernel mapping  $\mu_{v^*}$

---

**Input:** Voronoi sites  $Z^* = z_j^* (j \in [1, t], \text{Eq. 27})$  from the Alg. 1

STEP 0: Define initial  $Z^b = \{z_j^b\} = \{z_j^*\}$  and  $l_{previous} = 0$

STEP 1: **foreach**  $z_j^b \in Z^b$  **do**

Find most distant site  $z_m^b \in Z^b$

Generate tracer points:

$$\{\theta_{ij}^{tr}\} = \{\alpha_i \times z_j^b + (1 - \alpha_i) \times z_m^b\} \quad \alpha_i \in [0, 1] \forall i,$$

where  $i \in [1, n_{tr}]$  and  $n_{tr}$  is a number of tracers for each  $j$

STEP 2: Run the Algorithm 1 again in order to calculate iKernel mapping  $\psi(\theta_{ij}^{tr})$

STEP 3: To calculate the similarity between tracer points and maxima weighted iKernel mapping  $\mu_{v^*}$  (Fig. 5):

$$l(\theta_{ij}^{tr}, v^*) = \psi(\theta_{ij}^{tr})\mu_{v^*}$$

STEP 4: Extract tracers with maximal similarities:

$$\theta_k^{top}, k \in [1, k_{max}]$$

STEP 5: Using linear regression based on  $\theta_k^{top}$  get estimation of the parameter  $\theta^{est}$  with maximal similarity  $l_{max}$ .

STEP 6: **if**  $l_{max} - l_{previous} < \epsilon$  **then**

| STOP

**else**

$$l_{previous} = l_{max}$$

$$Z^b = \{z_k^b\} = \{\theta_k^{top}\}$$

| Goto STEP 1

**Result:**  $\theta^{est}$  and it's similarity  $l_{est} = \psi(\theta^{est})\mu_{v^*}$

---

## 4 Experiments

### 4.1 Synthetic data

To check the efficiency of the proposed algorithm we used many dimension data of two models: the first one is a gaussian function with unevenly distributed points with a gap at the center of distribution (region of interest); the second is a linear model with stochastic term  $\eta_{stoch}$  (see Application 2 for details). This research eschews the generation of new points and compares the methods based on a given sample of points using the mean squared error (MSE). The reason for this is just to avoid the effect of sampling methods and compare ABC methods based on an only given sample. That's why there are only 4 methods used for comparison: rejection ABC Pritchard *et al.* (1999) (Rejection in Fig. 4.2), ABC based on regression-based correction methods that use either local linear regression Beaumont *et al.* (2002) (Linear regression in Fig. 4.2) or neural networks (NN) Blum and François (2010) (Neural Network in Fig. 4.2). For calculations, we used the "abc" package in R that includes all methods above. The proposed method as well as kernel ABC based on Isolation Kernel denote in Fig. 4.2 as Maxima weighted and iKernel respectively.

All the results of synthetic experiments are presented in Application 2. For non-linear model of gaussian functions for each dimension iKernel ABC and ABC based on Maxima weighted iKernel mapping give a best values for all simulations with different dimensions (Maxima weighted iKernel mapping has usually accuracy that is better in 3.5 – 20 times than iKernel ABC (see Fig. 8)). Results for linear model depend on stochastic term: for  $\eta_{stoch} = 0$  linear regression gives absolutely exact values with  $MSE < 10^{-20}$ ; for  $\eta_{stoch} = 0.3$  and range of output  $Y \in [0, 10]$  ABC based on linear regression, NN and Maxima weighted iKernel mapping yield the results with similar MSE, iKernel and rejection ABC give MSE which is larger in several times; for  $\eta_{stoch} \geq 0.6$  (and the same output range) MSE for Maxima weighted iKernel mapping is the best for all cases (Fig. 4.2).

### 4.2 Cancer cell evolution

The most important part of tests is the model of a cancer cell evolution as an example of branching processes with a high probability of cell population extinction. In the research the tugHall simulator was used from work Nagornov and Kato (2020) as well as a dataset of simulations Nagornov *et al.* (2021). The model has 27 parameters, the 7 parameters of them were fixed because of expert estimation Nagornov and Kato (2020). The 20 parameters represent the hallmark - gene relationship that is analogue to gene-phenotype relations. Dataset has the results of the 9,600,000 simulations for different models, initial conditions and input parameters. Here the model with threshold metastatic transformation was used with the initial mutated cell in the pull of 1000 normal cells. This sample has the largest number of successful simulations equal 34,602 and non-zero outputs equal 34,059 of 400,000 simulations.

Based on the given sample of the dataset and VAF of a patient from The Cancer Genome Atlas (TCGA) database Hudson (Chairperson) as an observation (ID record is TCGA-AF-5654-01A-01D-1657-10), parameter estimation was performed by different methods. For rejection ABC, NN ABC and linear regression ABC, the mean, median as well as mode values were used for 100 times repetition of simulations for each parameter set. Unfortunately, only 1 value of the central tendencies gives the non-zero output for each method (denoted in the parentheses in Table 1) while the others lead to extinction for all the repetitions. That's why Table 1 shows results of simulations only for a successful attempt of the parameter set excluding iKernel ABC which also leads to extinction for all 100 simulations.

Observation data is a vector with 4 values VAF for each gene (APC, KRAS, TP53 and PIK3CA) related to colorectal cancer. There are corresponding distributions of simulations' output for each gene in the form of box plots in Application 3. Table 1 demonstrates statistical characteristics of the results of simulations for each method. Additional to MSE the part of succeeded simulations with survival cells is represented ( $\eta_{succeed}$ ). Standard deviation  $\sigma$  shows how the simulation data are concentrated around their center (for NN ABC  $\sigma = 0$  because of low probability of succeed simulations). Also, energy distance E-dist, as the statistical distance between observation and simulation, is included in Table 1 and was calculated using the 'energy' R package. Székely and Rizzo (2013, 2017).

According to Table 1 ABC based on Maxima weighted iKernel mapping gives the best accuracy. Rejection ABC and ABC based on correction with NN show the large mean squared error and high energy distance because they have good agreement with only VAF of PIK3CA gene (Fig. 13 of Application 3). The ABC based on correction with linear regression diverges with observation for VAF of APC gene (Fig. 10) that is the most frequent driver gene in colorectal cancer evolution

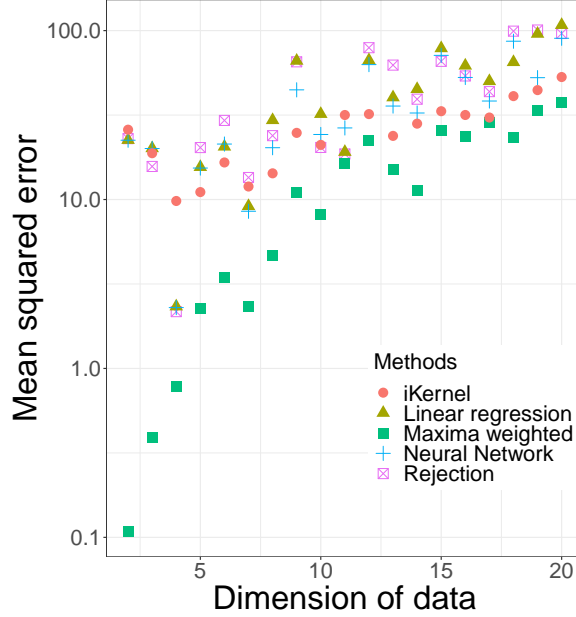


Figure 6: Mean squared error vs dimension of data with stochastic term  $\eta_{stoch} = 0.6$  from ABC estimations by different methods: linear regression, maxima weighted iKernel mapping, Isolation Kernel ABC, neural network and the rejection ABC.

Table 1: Statistics of simulation based on parameter estimation obtained by different methods:  $\eta_{succeed}$  is part of succeed simulation with non-zero output,  $\sigma$  is standard deviation, E-dist is energy distance.

Method	MSE	$\eta_{succeed}, \%$	$\sigma$	E-dist
Rejection (Median)	6956	38 %	212	1.616
Neural Network (Mean)	6999	7 %	0	1.464
Linear Regression (Mode)	1975	43 %	206	0.847
iKernel	×	×	×	×
Maxima weighted	68	52 %	97	0.086

Campbell *et al.* (2020). Only the proposed method gives a good agreement for VAF of all the genes (Figs. 10,11,12,13)

## 5 Conclusion

In this paper, we have developed heuristic ABC based on the part of Isolation kernel mapping with maximal weights  $\mu_{v^*}$  (Eqs. 25,26,27,28). Isolation kernel was realized with Voronoi diagram algorithm, that's why the explicit transformation of simulations' row-data to Hilbert space corresponding model's parameter is possible. In the simplest case, the interpretation of  $\mu_{v^*}$  is the intersection of all the Voronoi cells of  $\mu_{v^*}$  corresponding to observation point (Eq. 29).

The proposed method allows getting the parameter estimation with good accuracy even though the observation point lies in the sparse region of the given data sample. Maxima weighted iKernel mapping is also strong against the stochasticity of the simulation data as well as high dimensionality.

Application of the method to synthetic 2-20 dimension data with stochastic term and the tugHall simulator of cancer cell evolution shows much better results with comparison to well-known methods of ABC. The combination of Maxima weighted iKernel mapping with sampling techniques is one of the possible ways for a method's development.

### **Acknowledgements**

Author thanks Prof. Takashi Washio for detailed discussion of the theoretical part of the research as well as for the valuable critical comments.



## References

- Athreya, K. and Ney, P. (2012). *Branching Processes*. Grundlehren der mathematischen Wissenschaften. Springer Berlin Heidelberg.
- Aurenhammer, F. and Edelsbrunner, H. (1984). An optimal algorithm for constructing the weighted voronoi diagram in the plane. *Pattern Recognition*, **17**(2), 251–257.
- Beaumont, M. A., Zhang, W., and Balding, D. J. (2002). Approximate bayesian computation in population genetics. *Genetics*, **162**(4), 2025–2035.
- Bishop, C. M. (2006). *Pattern Recognition and Machine Learning*. Number 738p. Springer-Verlag New York.
- Blum, M. G. B. and François, O. (2010). Non-linear regression models for approximate bayesian computation. *Statistics and Computing*, **20**(1), 63–73.
- Borgwardt, K. M., Gretton, A., Rasch, M. J., Kriegel, H.-P., Schölkopf, B., and Smola, A. J. (2006). Integrating structured biological data by Kernel Maximum Mean Discrepancy. *Bioinformatics*, **22**(14), e49–e57.
- Burden, C. J. and Simon, H. (2016). Genetic drift in populations governed by a galton–watson branching process. *Theoretical Population Biology*, **109**, 63–74.
- Campbell, P. J., Getz, G., Korbelt, J. O., Stuart, J. M., Jennings, J. L., Stein, L. D., Perry, M. D., Nahal-Bose, H. K., Ouellette, B. F. F., Li, C. H., Rheinbay, E., Nielsen, G. P., Sgroi, D. C., Wu, C.-L., Faquin, W. C., Deshpande, V., Boutros, P. C., Lazar, A. J., Hoadley, K. A., Louis, D. N., Dursi, L. J., Yung, C. K., Bailey, M. H., Saksena, G., Raine, K. M., Buchhalter, I., Kleinheinz, K., Schlessner, M., Zhang, J., Wang, W., Wheeler, D. A., Ding, L., Simpson, J. T., O’Connor, B. D., Yakneen, S., Ellrott, K., Miyoshi, N., Butler, A. P., Royo, R., Shorsler, S. I., Vazquez, M., Rausch, T., Tiao, G., Waszak, S. M., Rodriguez-Martin, B., Shringarpure, S., Wu, D.-Y., Demidov, G. M., Delaneau, O., Hayashi, S., Imoto, S., Habermann, N., Segre, A. V., Garrison, E., Cafferkey, A., Alvarez, E. G., Heredia-Genestar, J., Muyas, F., Drechsel, O., Bruzos, A. L., Temes, J., Zamora, J., Baez-Ortega, A., Kim, H.-L., Mashl, R. J., Ye, K., DiBiase, A., Huang, K.-I., Letunic, I., McLellan, M. D., Newhouse, S. J., Shmaya, T., Kumar, S., Wedge, D. C., Wright, M. H., Yellapantula, V. D., Gerstein, M., Khurana, E., Marques-Bonet, T., Navarro, A., Bustamante, C. D., Siebert, R., Nakagawa, H., Easton, D. F., Ossowski, S., Tubio, J. M. C., De La Vega, F. M., Estivill, X., Yuen, D., Mihaiescu, G. L., Omberg, L., Ferretti, V., Sabarinathan, R., Pich, O., Gonzalez-Perez, A., Taylor-Weiner, A., Fittall, M. W., Demeulemeester, J., Tarabichi, M., Roberts, N. D., Van Loo, P., Cortés-Ciriano, I., Urban, L., Park, P., Zhu, B., Pitkänen, E., Li, Y., Saini, N., Klimczak, L. J., Weischenfeldt, J., Sidiropoulos, N., Alexandrov, L. B., Rabionet, R., Escaramis, G., Bosio, M., Holik, A. Z., Susak, H., Prasad, A., Erkek, S., Calabrese, C., Raeder, B., Harrington, E., Mayes, S., Turner, D., Juul, S., Roberts, S. A., Song, L., Koster, R., Mirabello, L., Hua, X., Tanskanen, T. J., Tojo, M., Chen, J., Aaltonen, L. A., Rättsch, G., Schwarz, R. F., Butte, A. J., Brazma, A., Chanock, S. J., Chatterjee, N., Stegle, O., Harismendy, O., Bova, G. S., Gordenin, D. A., Haan, D., Sieverling, L., Feuerbach, L., Chalmers, D., Joly, Y., Knoppers, B., Molnár-Gábor, F., Phillips, M., Thorogood, A., Townend, D., Goldman, M., Fonseca, N. A., Xiang, Q., Craft, B., Piñeiro-Yáñez, E., Muñoz, A., Petryszak, R., Füllgrabe, A., Al-Shahrour, F., Keays, M., Haussler, D., Weinstein, J., Huber, W., Valencia, A., Papatheodorou, I., Zhu, J., Fan, Y., Torrents, D., Bieg, M., Chen, K., Chong, Z., Cibulskis, K., Eils, R., Fulton, R. S., Gelpi, J. L., Gonzalez, S., Gut, I. G., Hach, F., Heinold, M., Hu, T., Huang, V., Hutter, B., Jäger, N., Jung, J., Kumar, Y., Lalansingh, C., Leshchiner, I., Livitz, D., Ma, E. Z., Maruvka, Y. E., Milovanovic, A., Nielsen, M. M., Paramasivam, N., Pedersen, J. S., Puiggròs, M., Sahinalp, S. C., Sarrafí, I., Stewart, C., Stobbe, M. D., Wala, J. A., Wang, J., Wendl, M., Werner, J., Wu, Z., Xue, H., Yamaguchi, T. N., Yellapantula, V., Davis-Dusenbery, B. N., Grossman, R. L., Kim, Y., Heinold, M. C., Hinton, J., Jones, D. R., Menzies, A., Stebbings, L., Hess, J. M., Rosenberg, M., Dunford, A. J., Gupta, M., Imielinski, M., Meyerson, M., Beroukhim, R., Reimand, J., Dhingra, P., Favero, F., Dentre, S., Wintersinger, J., Rudneva, V., Park, J. W., Hong, E. P., Heo, S. G., Kahles, A., Lehmann, K.-V., Soulette, C. M., Shiraishi, Y., Liu, F., He, Y., Demircioğlu, D., Davidson, N. R., Greger, L., Li, S., Liu, D., Stark, S. G., Zhang, F., Amin, S. B., Bailey, P., Chateigner, A., Frenkel-Morgenstern, M., Hou, Y., Huska, M. R., Kilpinen, H., Lamaze, F. C., Li, C., Li, X., Li, X., Liu, X., Marin, M. G., Markowski, J., Nandi, T., Ojesina, A. I., Pan-Hammarström, Q., Park, P. J., Pedamallu, C. S., Su, H., Tan, P., Teh, B. T., Wang, J., Xiong, H., Ye, C., Yung, C., Zhang, X., Zheng, L., Zhu, S., Awadalla, P., Creighton, C. J., Wu, K., Yang, H., Göke, J., Zhang, Z., Brooks, A. N., Fittall, M. W., Martincorena, I., Rubio-Perez, C., Juul, M., Schumacher, S., Shapira, O., Tamborero, D., Mularoni, L., Hornshøj, H., Deu-Pons, J., Muiños, F., Bertl, J., Guo, Q., and of Whole Genomes Consortium, T. I. P.-C. A. (2020). Pan-cancer analysis of whole genomes. *Nature*, **578**(7793), 82–93.
- Chen, Y. and Welling, M. (2010). Parametric herding. In Y. W. Teh and M. Titterton, editors, *Proceedings of the Thirteenth International Conference on Artificial Intelligence and Statistics*, volume 9 of *Proceedings of Machine Learning Research*, pages 97–104, Chia Laguna Resort, Sardinia, Italy. PMLR.
- Chen, Y., Welling, M., and Smola, A. (2010). Super-samples from kernel herding. In *Proceedings of the Twenty-Sixth Conference on Uncertainty in Artificial Intelligence*, UAI’10, pages 109–116, Arlington, Virginia, USA. AUAI Press.
- Chen, Y., Tong, D., and Wu, C.-I. (2017). A New Formulation of Random Genetic Drift and Its Application to the Evolution of Cell Populations. *Molecular Biology and Evolution*, **34**(8), 2057–2064.
- Csillery, K., Blum, M. G., Gaggiotti, O. E., and François, O. (2010). Approximate bayesian computation (abc) in practice. *Trends in Ecology and Evolution*, **25**(7), 410–418.
- Devroye, L. (1998). *Branching Processes and Their Applications in the Analysis of Tree Structures and Tree Algorithms*, pages 249–314. Springer Berlin Heidelberg, Berlin, Heidelberg.
- Dyer, M., Frieze, A., and Kannan, R. (1991). A random polynomial-time algorithm for approximating the volume of convex bodies. *J. ACM*, **38**(1), 1–17.
- Fortune, S. (1987). A sweepline algorithm for voronoi diagrams. *Algorithmica*, **2**(1), 153.
- Fukumizu, K., Gretton, A., Sun, X., and Schölkopf, B. (2008). Kernel measures of conditional dependence. In J. Platt, D. Koller, Y. Singer, and S. Roweis, editors, *Advances in Neural Information Processing Systems*, volume 20. Curran Associates, Inc.
- Fukumizu, K., Song, L., and Gretton, A. (2013). Kernel bayes’ rule: Bayesian inference with positive definite kernels. *J. Mach. Learn. Res.*, **14**(1), 3753–3783.
- Gelb, P., Klus, S., Schuster, I., and Schutte, C. (2021). Feature space approximation for kernel-based supervised learning. *Knowledge-Based Systems*, **221**, 106935.

- Gretton, A., Borgwardt, K. M., Rasch, M. J., Schölkopf, B., and Smola, A. (2012). A kernel two-sample test. *J. Mach. Learn. Res.*, **13**(null), 723–773.
- Huang, L., Huang, S., and Lai, Z. (2020). On the optimization of site investigation programs using centroidal voronoi tessellation and random field theory. *Computers and Geotechnics*, **118**, 103331.
- Hudson (Chairperson), T. J., Anderson, W., Aretz, A., Barker, A. D., Bell, C., Bernabé, R. R., Bhan, M. K., Calvo, F., Eerola, I., Gerhard, D. S., Guttmacher, A., Guyer, M., Hemsley, F. M., Jennings, J. L., Kerr, D., Klatt, P., Kolar, P., Kusuda, J., Lane, D. P., Laplace, F., Lu, Y., Nettekoven, G., Ozenberger, B., Peterson, J., Rao, T. S., Remacle, J., Schafer, A. J., Shibata, T., Stratton, M. R., Vockley, J. G., Watanabe, K., Yang, H., Yuen, M. M. F., Knoppers (Leader), B. M., Bobrow, M., Cambon-Thomsen, A., Dressler, L. G., Dyke, S. O. M., Joly, Y., Kato, K., Kennedy, K. L., Nicolás, P., Parker, M. J., Rial-Sebbag, E., Romeo-Casabona, C. M., Shaw, K. M., Wallace, S., Wiesner, G. L., Zeps, N., Lichter (Leader), P., Biankin, A. V., Chabannon, C., Chin, L., Clément, B., de Alava, E., Degos, F., Ferguson, M. L., Geary, P., Hayes, D. N., Hudson, T. J., Johns, A. L., Kasprzyk, A., Nakagawa, H., Penny, R., Piris, M. A., Sarin, R., Scarpa, A., van de Vijver, M., Futreal (Leader), P. A., Aburatani, H., Bayés, M., Bowtell, D. D. L., Campbell, P. J., Estivill, X., Gerhard, D. S., Grimmond, S. M., Gut, I., Hirst, M., López-Otín, C., Majumder, P., Marra, M., McPherson, J. D., Ning, Z., Puente, X. S., Ruan, Y., Stratton, M. R., Stunnenberg, H. G., Swerdlow, H., Velculescu, V. E., Wilson, R. K., Xue, H. H., Yang, L., Spellman (Leader), P. T., Bader, G. D., Boutros, P. C., Campbell, P. J., Flicek, P., Getz, G., Guigó, R., Guo, G., Haussler, D., Heath, S., Hubbard, T. J., Jiang, T., Jones, S. M., Li, Q., López-Bigas, N., Luo, R., Muthuswamy, L., Francis Ouéllette, B. F., Pearson, J. V., Puente, X. S., Quesada, V., Raphael, B. J., Sander, C., Speed, T. P., Stein, L. D., Stuart, J. M., Teague, J. W., Totoki, Y., Tsunoda, T., Valencia, A., Wheeler, D. A., Wu, H., Zhao, S., Zhou, G., Stein (Leader), L. D., Hubbard, T. J., Jones, S. M., Lathrop, M., Francis Ouéllette, B. F., Spellman, P. T., Teague, J. W., Thomas, G., Yoshida, T., Kennedy (Leader), K. L., Axton, M., Dyke, S. O. M., Futreal, P. A., Gerhard, D. S., Gunter, C., Hudson, T. J., McPherson, J. D., Miller, L. J., Shaw, K. M., Kasprzyk (Leader), A., Stein (Leader), L. D., Zhang, J., Haider, S. A., Wang, J., Yung, C. K., Cross, A., Liang, Y., Gnaneshan, S., Guberman, J., Hsu, J., Bobrow (Leader), M., Chalmers, D. R. C., Hasel, K. W., Kaan, T. S. H., Kennedy, K. L., Knoppers, B. M., Lowrance, W. W., Masui, T., Lyman Rodriguez, L., Vergely, C., Grimmond (Leader), S. M., Biankin, A. V., Bowtell, D. D. L., Cloonan, N., deFazio, A., Eshleman, J. R., Etemadmoghadam, D., Gardiner, B. A., Kench, J. G., Sutherland, R. L., Tempero, M. A., Waddell, N. J., Wilson, P. J., McPherson (Leader), J. D., Gallinger, S., Tsao, M.-S., Shaw, P. A., Petersen, G. M., Mukhopadhyay, D., DePinho, R. A., Thayer, S., Shazand, K., Beck, T., Sam, M., Timms, L., Ballin, V., Lu (Leader), Y., Ji, J., Zhang, X., Chen, F., Hu, X., Yang, Q., Tian, G., Zhang, L., Xing, X., Li, X., Zhu, Z., Yu, Y., Yu, J., Lathrop (Leader), M., Tost, J., Brennan, P., Holcatova, I., Zaridze, D., Brazma, A., Egevad, L., Prokhorchouk, E., Elizabeth Banks, R., Uhlén, M., Viksna, J., Ponten, F., Skryabin, K., Stratton (Leader), M. R., Futreal, P. A., Birney, E., Borg, A., Børresen-Dale, A.-L., Caldas, C., Foekens, J. A., Martin, S., Reis-Filho, J. S., Richardson, A. L., Sotiriou, C., Stunnenberg, H. G., van't Veer, L., Calvo (Leader), F., Birnbaum, D., Blanche, H., Boucher, P., Boyault, S., Masson-Jacquemier, J. D., Pauporté, I., Pivot, X., Vincent-Salomon, A., Tabone, E., Theillet, C., Treilleux, I., Bioulac-Sage, P., Decaens, T., Franco, D., Gut, M., Samuel, D., Consortium, T. I. C. G., committee, E., Ethics, policy committee, Tissue, clinical annotation working group, working group, T., analyses working group, B., coordination, D., management working group, Data release, d. t., publications working group, coordination centre, D., data access committee, I., genome projects: Pancreatic cancer (ductal adenocarcinoma), C., ovarian cancer (serous adenocarcinoma) (Australia), cancer (ductal adenocarcinomas) (Canada), P., cancer (intestinal, G., diffuse-type) (China), cancer (renal cell carcinoma; focus on but not limited to clear cell subtype) (European Union/France), R., cancer (subtypes defined by an amplification of ER+ HER ductal-type) (European Union/United Kingdom), B., cancer (subtype defined by an amplification of the HER2 gene) (France), B., cancer (hepatocellular carcinoma; secondary to alcohol, L., and adiposity) (France) (2010). International network of cancer genome projects. *Nature*, **464**(7291), 993–998.
- Jagers, P. (1989). General branching processes as markov fields. *Stochastic Processes and their Applications*, **32**(2), 183–212.
- Kajihara, T., Kanagawa, M., Yamazaki, K., and Fukumizu, K. (2018). Kernel recursive ABC: Point estimation with intractable likelihood. In J. Dy and A. Krause, editors, *Proceedings of the 35th International Conference on Machine Learning*, volume 80 of *Proceedings of Machine Learning Research*, pages 2400–2409. PMLR.
- Lacoste-Julien, S., Lindsten, F., and Bach, F. R. (2015). Sequential kernel herding: Frank-wolfe optimization for particle filtering. *ArXiv*, **abs/1501.02056**.
- Liu, F. T., Ting, K. M., and Zhou, Z.-H. (2008). Isolation forest. In *2008 Eighth IEEE International Conference on Data Mining*, pages 413–422.
- Liu, F. T., Ting, K. M., and Zhou, Z.-H. (2012). Isolation-based anomaly detection. *ACM Trans. Knowl. Discov. Data*, **6**(1).
- Liu, J. S. and Chen, R. (1998). Sequential monte carlo methods for dynamic systems. *Journal of the American Statistical Association*, **93**(443), 1032–1044.
- Muandet, K., Fukumizu, K., Sriperumbudur, B., and Schölkopf, B. (2017). Kernel mean embedding of distributions: A review and beyond. *Foundations and Trends® in Machine Learning*, **10**(1-2), 1–141.
- Nagornov, I. S. and Kato, M. (2020). tugHall: a simulator of cancer-cell evolution based on the hallmarks of cancer and tumor-related genes. *Bioinformatics*, **36**(11), 3597–3599.
- Nagornov, I. S., Nishino, J., and Kato, M. (2021). Dataset of tughall simulations of cell evolution for colorectal cancer. *Data in Brief*, **34**, 106719.
- Nakagome, S., Fukumizu, K., and Mano, S. (2013). Kernel approximate bayesian computation in population genetic inferences. *Statistical Applications in Genetics and Molecular Biology*, **12**(6), 667–678.
- Park, M., Jitkrittum, W., and Sejdinovic, D. (2016). K2-abc: Approximate bayesian computation with kernel embeddings. In A. Gretton and C. C. Robert, editors, *Proceedings of the 19th International Conference on Artificial Intelligence and Statistics*, volume 51 of *Proceedings of Machine Learning Research*, pages 398–407, Cadiz, Spain. PMLR.
- Pritchard, J. K., Seielstad, M. T., Perez-Lezaun, A., and Feldman, M. W. (1999). Population growth of human Y chromosomes: a study of Y chromosome microsatellites. *Molecular Biology and Evolution*, **16**(12), 1791–1798.
- Székely, G. J. and Rizzo, M. L. (2013). Energy statistics: A class of statistics based on distances. *Journal of Statistical Planning and Inference*, **143**(8), 1249–1272.
- Székely, G. J. and Rizzo, M. L. (2017). The energy of data. *Annual Review of Statistics and Its Application*, **4**(1), 447–479.

- Ting, K. M., Zhu, Y., and Zhou, Z.-H. (2018). Isolation kernel and its effect on svm. In *Proceedings of the 24th ACM SIGKDD International Conference on Knowledge Discovery and Data Mining*, KDD '18, pages 2329–2337, New York, NY, USA. Association for Computing Machinery.
- Ting, K. M., Xu, B.-C., Washio, T., and Zhou, Z.-H. (2020). Isolation distributional kernel: A new tool for kernel based anomaly detection. In *Proceedings of the 26th ACM SIGKDD International Conference on Knowledge Discovery and Data Mining*, KDD '20, pages 198–206, New York, NY, USA. Association for Computing Machinery.
- Ting, K. M., Washio, T., Zhu, Y., and Xu, Y. (2021). Breaking the curse of dimensionality with isolation kernel.
- Wan, S., Zhao, Y., Wang, T., Gu, Z., Abbasi, Q. H., and Choo, K.-K. R. (2019). Multi-dimensional data indexing and range query processing via voronoi diagram for internet of things. *Future Generation Computer Systems*, **91**, 382–391.
- Wasserman, L. (2010). *All of Statistics: A Concise Course in Statistical Inference*. pringer Publishing Company, Incorporated.
- West, J., Hasnain, Z., Macklin, P., and Newton, P. K. (2016). An evolutionary model of tumor cell kinetics and the emergence of molecular heterogeneity driving gompertzian growth. *SIAM Review*, **58**(4), 716–736.
- Williams, M. J., Werner, B., Heide, T., Curtis, C., Barnes, C. P., Sottoriva, A., and Graham, T. A. (2018). Quantification of subclonal selection in cancer from bulk sequencing data. *Nature Genetics*, **50**(6), 895–903.

## Application 1. Isolation Forest

The Isolation Forest (iForest) algorithm was initially proposed in the papers Liu *et al.* (2012, 2008). The authors defined anomalous data points as the points in a sparse region of dataset  $D \in R^d$  in comparison with normal points which are in a dense region. Since anomalies are in sparse area, they are easier to “isolate” compared to normal points. Isolation Forest builds an ensemble of Isolation Trees (*iTrees*) based on many subsets  $\mathcal{D}_i \subset D$ , and anomalies are the all points  $x \in D$  of whole dataset  $D$  that have shorter average path lengths  $\hat{h}(x)$  on the *iTrees*.

In the paper Liu *et al.* (2012) the authors described a set of experiments to prove that iForest:

- has a low linear time complexity and a small memory requirement due to small size  $\xi = |\mathcal{D}|$  of subsets  $\mathcal{D}_i, i \in [1..t]$  and finite number of *iTrees*  $t$ ;
- is able to deal with high dimensional data  $\mathcal{D} \in R^d$ , where  $d$  is number of dimensions;
- can be trained with or without anomalies in the **Training Set** =  $\bigcup_{i=1}^t \mathcal{D}_i$ ;
- can provide detection results with different levels of granularity without re-training at the **Evaluation stage**.

In order to isolate a data point the algorithm of iForest (Algorithm 3) recursively generates partitions  $\mathcal{H}_i$  on the sample  $\mathcal{D}_i$  by randomly selecting an attribute  $q \in [1..d]$  and then randomly selecting a split value  $p$  for the attribute, between the minimum  $q_{min}$  and maximum  $q_{max}$  values allowed for that attribute.

*iTree<sub>k</sub>* at **training step**  $k$  has an information on recursive partitioning  $\mathcal{H}_k$ . The length of the path  $h_k(x)$  in the *iTree<sub>k</sub>* is defined as the number of partitions required to isolate a point  $x$  within the tree *iTree<sub>k</sub>*, to reach a terminating leaf-node starting from the root-node. Let  $D = \{x_1, \dots, x_n\} \in R^d$  be a set of  $d$ -dimensional points,  $\mathcal{D} = \{z_1, z_2, \dots, z_\xi\}, \mathcal{D} \subset D$  be a subset of  $D$  with a size of subset  $|\mathcal{D}| = \xi \ll n$ . Thus *iTree* is defined as a data structure with the following properties:

- for each node  $V$  in the *iTree*,  $V$  is either an leaf-node with no child, or an branching-node with one partition and exactly two daughter nodes ( $V_l, V_r$  - left and rights branches respectively).
- a partition at node  $V$  consists of an attribute  $q$  and a splitting value  $p$  such that condition of  $x^q < p$  determines the traversal of a data point  $x$  to left branch  $V_l$  and otherwise to right branch  $V_r$ .

---

### Algorithm 3: Isolation Forest algorithm to detect anomalies

---

**Data:** Multidimensional Dataset  $D = \{x_1, x_2, \dots, x_n\} \in R^d$

**Input:**  $t$  - number of trees,  $\xi$  - subsampling size,  $\xi \ll n$

#### I) Training Stage

**for**  $k = 1 .. t$  **do**

**Make Isolation Tree** *iTree<sub>k</sub>*:

Randomly get subset  $\mathcal{D} \subset D$ , where  $\mathcal{D} = \{z_1, z_2, \dots, z_j, \dots, z_\xi\}$

Randomly split space  $R^d$  by partitions  $\mathcal{H}_k$

until all  $z_j \in \mathcal{D}$  will be isolated [based on *iTree* algorithm]

*iTree<sub>k</sub>* = a tree of partitions  $\mathcal{H}_k$

**Output:** Isolation Forest = a set of *iTree<sub>k</sub>*, where  $k \in [1..t]$

#### II) Evaluation Stage

**foreach**  $x \in D$  **do**

**for**  $k = 1 .. t$  **do**

find corresponded leaf-node for  $x$  in *iTree<sub>k</sub>*

calculate  $h_k(x)$  - length of path in *iTree<sub>k</sub>*

find average  $\hat{h}(x) = \frac{1}{t} \sum_{k=1}^t h_k(x)$

**Result:**  $\hat{h}(x)$  - average path length in the iForest

---

In order to build an *iTree*, the algorithm recursively divides subset  $\mathcal{D}$  by randomly selecting an attribute  $q$  and a split value  $p$ , until either (i) the node has only one point or (ii) all points at node have the same coordinates. Once each point in subset  $\mathcal{D}$  is isolated at one of the leaf-nodes, *iTree* is fully grown and **training stage** is finished.

Algorithm 3 shows two stages of Isolation Forest - training and evaluation stages. It’s clear that the anomalous points are those with the smaller path length in the tree, where the path length  $h(x_i)$

of point  $x_i \in D$  is defined as the number of edges  $x_i$  traverses from the root vertex to get to a leaf-node. Algorithm 3 shows that the training stage is needed to construct the  $t$  *iTrees* for  $t$  subsets  $\mathcal{D}_k, k \in [1..t]$ . Set of *iTrees* is Isolation Forest. During Evaluation stage iForest measures the path length in each *iTree*  $h_k(x), k = [1..t]$  for each point  $x \in D$ .

## Application 2. Results of synthetic simulation

For synthetic simulations we used many dimension data of two models based on linear and gaussian functions. Each model has a dimension  $d \in [2, 20]$ , input parameter  $X = \{x_1, \dots, x_d\}$  and output data with same dimensionality  $Y = \{y_1, \dots, y_d\}$ . To simplify consideration of the results we define each element of output vector as function of only one input variable  $y_i = f(x_i)$ , where  $i \in [1..d]$ . For each model it should be found the values of parameters  $x_{01}, \dots, x_{0d}$ . Thus, the linear model is defined as:

$$Y_{lin}(X) = \left\{ \begin{array}{l} \alpha_1 \cdot (x_1 - x_{01}) + \eta_{1,stoich}, \\ \dots, \\ \alpha_i \cdot (x_i - x_{0i}) + \eta_{i,stoich}, \\ \dots, \\ \alpha_d \cdot (x_d - x_{0d}) + \eta_{d,stoich} \end{array} \right\} \quad (32)$$

where  $\eta_{i,stoich}$  is a stochastic term of  $i^{th}$  dimension.

The second model is based on gaussian functions:

$$Y_{Gauss}(X) = \left\{ \begin{array}{l} e^{-\alpha_1 \cdot (x_1 - x_{01})^2}, \\ \dots, \\ e^{-\alpha_i \cdot (x_i - x_{0i})^2}, \\ \dots, \\ e^{-\alpha_d \cdot (x_d - x_{0d})^2} \end{array} \right\} \quad (33)$$

Number of points in the sample depends on distance to point of interest  $x_{0i}$  (see Fig. 7, for example) to prepare sparse regions and imitate the lack of information around the observation point.

We used 4 methods to get parameter estimation: rejection ABC Pritchard *et al.* (1999) (Rejection in Figs. 8 and 9), ABC based on regression-based correction methods that use either local linear regression Beaumont *et al.* (2002) (Linear regression in Figs. 8 and 9) or neural networks Blum and François (2010) (Neural Network in in Figs. 8 and 9). Implementation of calculation was done using the "abc" package in R with default values. Also, we tried to adjust internal parameters to improve the results but that's redundant for these toy tasks. The proposed method as well as kernel ABC based on Isolation Kernel denote in Figs. 8 and 9) as Maxima weighted and iKernel respectively.

For non-linear model of gaussian functions for each dimension iKernel ABC and ABC based on Maxima weighted iKernel mapping give a best values for all simulations with different dimensions (Maxima weighted iKernel mapping has usually accuracy that is better in 3.5 – 20 times than iKernel ABC (see Fig. 8) excluding a few points). The worst values of MSE are given by ABC based on linear regression because the model is significant non-linear.

Results for linear model depend on stochastic term: for  $\eta_{stoich} = 0$  linear regression gives absolutely exact values with  $MSE < 10^{-20}$ ; for  $\eta_{stoich} = 0.3$  and range of output  $Y \in [0, 10]$  ABC based on linear regression, NN and Maxima weighted iKernel mapping yield the results with similar MSE(Fig. 9), iKernel and rejection ABC give MSE which is larger in several times; for  $\eta_{stoich} \geq 0.6$  (and the same output range) MSE for Maxima weighted iKernel mapping is the best for all cases (Fig. 4.2). Unfortunately, iKernel ABC shows an accuracy similar with rejection algorithm that's why one may expect the same behavior for cancer simulation case.

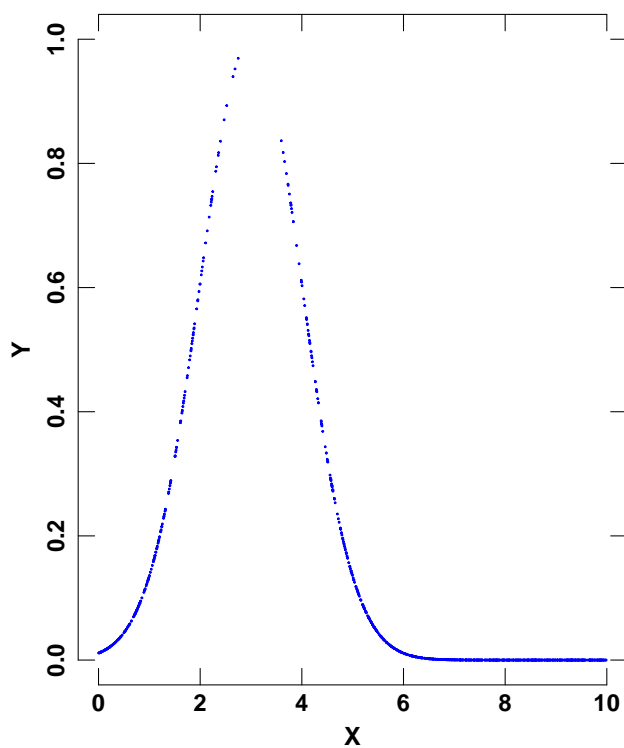


Figure 7: Row data for model with gaussian function and lower probability of generation at the maximum (point of interest).

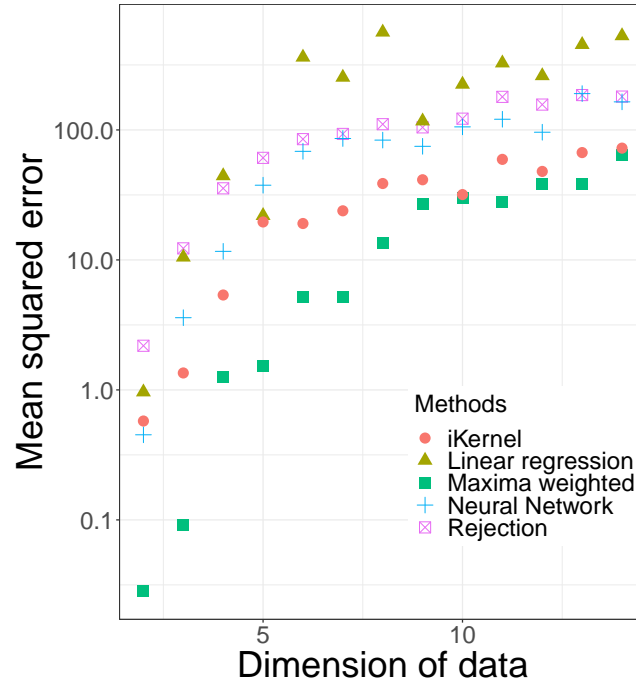


Figure 8: Mean squared error vs dimension of data for the model based on gaussian function from ABC estimations by different methods: linear regression, maxima weighted iKernel mapping, Isolation Kernel ABC, neural network and the rejection ABC.

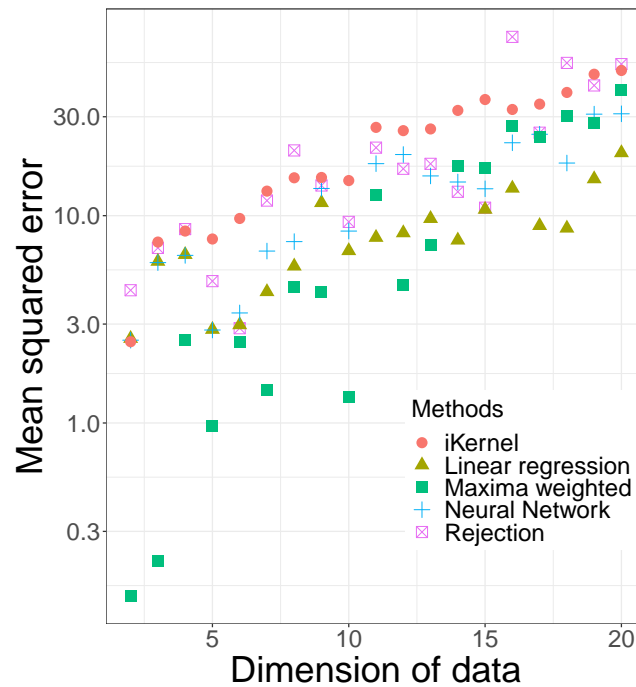


Figure 9: Mean squared error vs dimension of data for linear model with stochastic term  $\eta_{stoch} = 0.3$  from ABC estimations by different methods: linear regression, maxima weighted iKernel mapping, Isolation Kernel ABC, neural network and the rejection ABC.



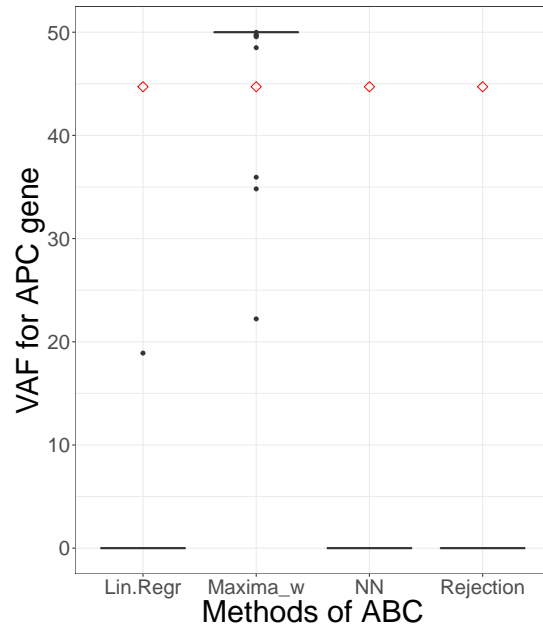
**Application 3. Box plots of the results of simulations of cancer cell evolution**

Figure 10: Box plot of VAF of APC gene gotten by different methods as well as observation point (diamond).

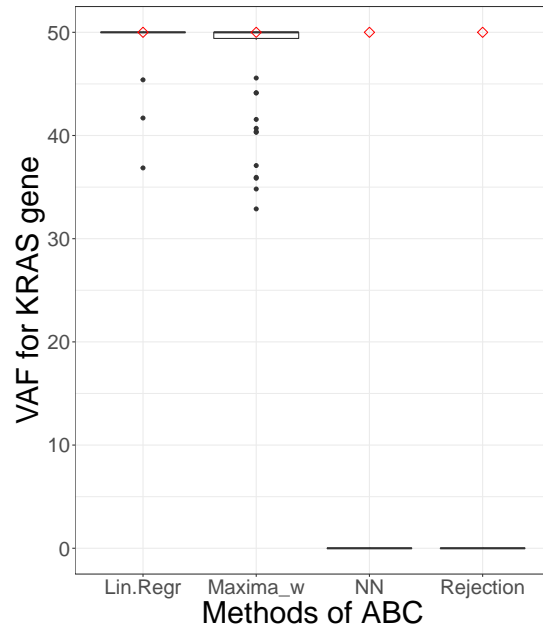


Figure 11: Box plot of VAF of KRAS gene gotten by different methods as well as observation point (diamond).

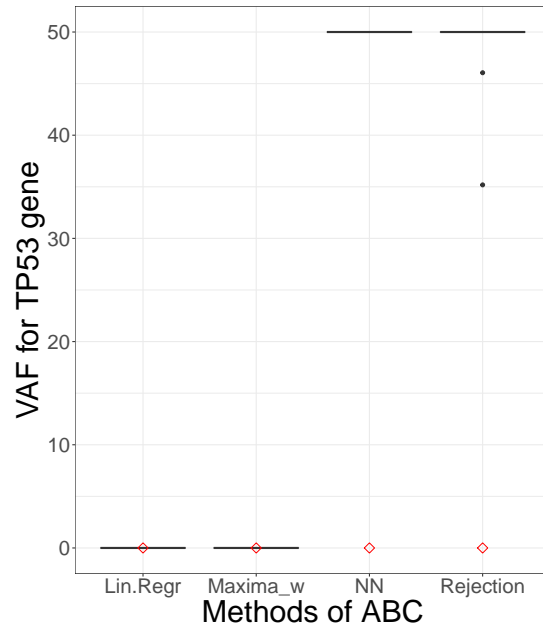


Figure 12: Box plot of VAF of TP53 gene gotten by different methods as well as observation point (diamond).

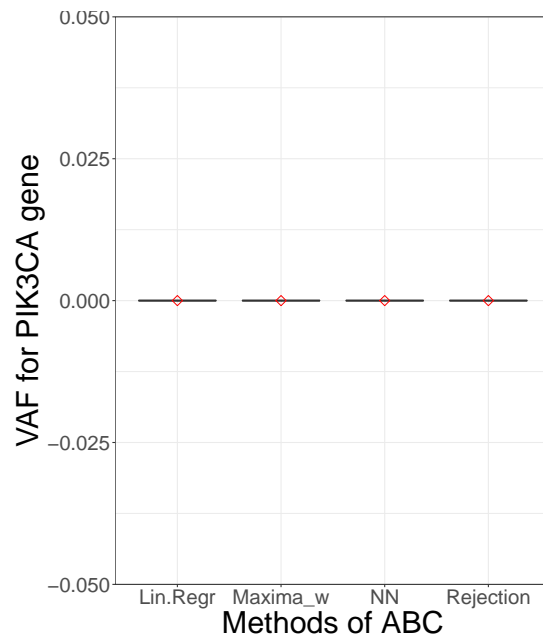


Figure 13: Box plot of VAF of PIK3CA gene gotten by different methods as well as observation point (diamond).